Biochemistry

 Volume 20, Number 10 May 12, 1981

Kinetics of pH-Dependent Interconversion of Tryptophanase Spectral Forms Studied by Scanning Stopped-Flow Spectrophotometry†

David S. June,‡ Clarence H. Suelter,* and James L. Dye

ABSTRACT: Morino and Snell [Morino, Y., & Snell, E. E. (1967) *J. Biol. Chem. 242*, 5591–5601] previously showed that the relative amplitudes of the 337- and 420-nm absorption bands of tryptophanase depended on both pH and the nature of a required monovalent cation activator. An investigation of the kinetics of interconversion of the 337- and 420-nm forms following a rapid incremental increase (jump) or decrease (drop) in pH over the range of enzyme stability in 0.2 M KCl at 24 ± 0.3 °C by scanning stopped-flow spectrophotometry showed three distinct time-dependent phases. They were (1) an abrupt phase which is complete in <6.5 ms, (2) a fast first-order interconversion of the 420- and 337-nm absorbances, and (3) a slow first-order process involving growth at 355 nm coupled to two decays centered at 325 and 430 nm in the incremental pH jumps and decay at 355 nm with concomitant growth at 430 and 290 nm in the incremental pH-drop experiments. The results of these experiments were analyzed in terms of a scheme involving enzyme forms E_α, E_β, $E_\beta H^+$, E_γ, $E_\gamma H^+$, and E_δ. The E_α form predominates in the absence of activating monovalent cations and absorbs at 420 nm. Those in the β manifold, E_β and $E_\beta H^+$, also absorb at 420 nm while those in the γ manifold, E_γ and $E_\gamma H^+$, absorb at 337 nm. The form E_δ absorbs at 355 nm. $E_\beta H^+$ and $E_\gamma H^+$ represent the protonated form of the enzyme in each manifold. Analysis of the abrupt phase showed no significant systematic changes in absorbance above 330 nm for either the pH-jump or pH-drop experiments. The fast second phase involves the first-order interconversion of the β and γ manifolds while the slow third phase describes the buildup or decay of the δ manifold. Presumably conformational changes control the rate of these interconversions. The pH dependence of the fast first-order β to γ conversion was described and evaluated in terms of five independent equilibrium and rate constants and three independent amplitude terms by simultaneously fitting the amplitude data and first-order rate constants to an equation describing the overall scheme with a nonlinear least-squares program KINFIT4 [Dye, J. L., & Nicely, V. A. (1971) *J. Chem. Educ. 48*, 443–448]. The pK for protonation of the β form = 9.70 ± 0.12, for protonation of the γ form (337-nm absorber) = 6.77 ± 0.10, and for the pH-dependent interconversion of the β and γ manifolds, pK_a = 8.11 ± 0.04. The computed equilibrium distribution among the four species of the β and γ manifolds showed that $E_\beta H^+$ and E_γ predominate.

Tryptophanase from *Escherchia coli* B/1t7-A is a pyridoxal-P[1] dependent enzyme that catalyzes α,β-elimination reactions of amino acid substrates and requires monovalent cations for optimum activity (Snell, 1975). Since no previous studies have dealt directly with the pre-steady-state and steady-state kinetics of the tryptophanase reaction, we initiated such a study in an effort to deduce the mechanism of the reaction and the role of monovalent cations in this reaction.

Tryptophanase has two absorption maxima above 280 nm centered at 337 and 420 nm, and their relative amplitudes depend on both pH and monovalent cations (Morino & Snell, 1967). We reported previously (June et al., 1979) that the 420- and 337-nm forms of the enzyme interconvert in a complex fashion on the stopped-flow time scale following a rapid change in pH or monovalent cation concentration. As a prelude to a study of the interaction of substrates with the enzyme, we have extended the pH-dependent 420–337-nm interconversions by examining incremental pH jumps and drops in the scanning stopped-flow spectrophotometer over the range of enzyme stability. Major features of the data are interpreted in terms of a scheme which includes equilibrium and rate constants and postulated structures of the coenzyme that may be involved in the spectral changes. The results of a study of the interaction of inhibitors with the enzyme are presented in an accompanying paper (June et al., 1981).

Materials and Methods

Materials. KCl was Mallinckrodt, analytical reagent grade. 2-(*N*-Morpholino)ethanesulfonic acid (Mes),[1] *N*-tris(hydroxymethyl)methyl-2-aminoethanesulfonic acid (Tes), *N*-(2-

† From the Department of Biochemistry (C.H.S.) and the Department of Chemistry (J.L.D.), Michigan State University, East Lansing, Michigan 48824. *Received April 28, 1980.* This work was supported by National Science Foundation Grant PCM 78-18905.

‡ Present address: Marion Laboratories, Kansas City, MO 64137.

[1] Abbreviations used: Mes, 2-(*N*-morpholino)ethanesulfonic acid; Tes, *N*-tris(hydroxymethyl)methyl-2-aminoethanesulfonic acid; Bicine, *N,N*-bis(2-hydroxyethyl)glycine; pyridoxal-P, pyridoxal 5′-phosphate; DTT, DL-dithiothreitol; SOPC, *S*-(*o*-nitrophenyl)-L-cysteine; EDTA, ethylenediaminetetraacetic acid.

0006-2960/81/0420-2707$01.25/0

hydroxyethyl)piperazinepropanesulfonic acid (Hepps), *N,N*-bis(2-hydroxyethyl)glycine (Bicine), pyridoxal 5′-phosphate, and DL-dithiothreitol (DTT) were obtained from Sigma Chemical Co.

Tryptophanase. Tryptophanase was prepared according to the method of Suelter et al. (1977). Stock apoenzyme was activated by incubation for 1 h at 37 °C in 0.1 M potassium phosphate, pH 8.0, 1 mM EDTA, 7% $(NH_4)_2SO_4$, 0.2 mM pyridoxal-P, and 20 mM DTT. The enzyme had a specific activity of 50–55 μmol min^{-1} mg^{-1} when assayed at 30 °C with 0.6 mM *S*-(*o*-nitrophenyl)-L-cysteine (SOPC) in 50 mM potassium phosphate, pH 8.0, and 50 mM KCl (Suelter et al., 1976). Protein concentration was determined spectrophotometrically by using ϵ_{278} = 0.795 mL mg^{-1} cm^{-1} (Hogberg-Raibaud et al., 1975).

Incremental pH-Jump Experiments. Activated holotryptophanase (~20 mg mL^{-1}) was equilibrated with 1 mM Tes, pH 7.00, 0.2 M KCl, 15 μM pyridoxal-P, 1 mM EDTA, and 0.2 mM DTT by dialysis at 4 °C. Prior to use, the enzyme was diluted to a concentration of 2.9 mg mL^{-1} with the dialysis buffer. This solution was pushed against 50 mM bicine, pH_i, 0.2 M KCl, 15 μM pyridoxal-P, and 1 mM EDTA to give the final pH values of 7.69, 8.07, 8.56, 8.90, and 9.33.

Incremental pH-Drop Experiments. Activated holotryptophanase (~20 mg mL^{-1}) was equilibrated with 1 mM Bicine, pH 8.70, 0.2 M KCl, 15 μM pyridoxal-P, 1 mM EDTA, and 0.2 mM DTT by dialysis at 4 °C. The enzyme was diluted with the dialysis buffer to a concentration of 4.0 mg mL^{-1} prior to the experiment. This solution was pushed against 50 mM Tes, pH_i, 0.2 M KCl, 15 μM pyridoxal-P, and 1 mM EDTA to give final pH values of 6.54, 7.03, 7.47, 7.77, 8.25, and 8.44.

Scanning Stopped-Flow Experiments. Stopped-flow data were collected at 24.0 ± 0.3 °C on a scanning instrument described elsewhere (Coolen et al., 1975; Papadakis et al., 1975). Seventy-five spectra were collected/s, each requiring 6.7 ms, over the wavelength range 280–550 nm for a period of 65 s in the pH-jump experiments and 111 s in the pH-drop experiments. A total of 50 and 56 spectra were stored in the pH-jump and pH-drop experiments, respectively, by using an averaging scheme outlined previously (Suelter et al., 1975). Control spectra were collected as described previously (June et al., 1979).

Data Analysis. Data were fit with the appropriate mathematical function by using the nonlinear curve-fitting program KINFIT4 (Dye & Nicely, 1971). Errors listed are marginal standard deviations and therefore include the effect of "coupling" among the parameters. The raw data, consisting of absorbance vs. time at any of 60 wavelength channels following a pH jump or drop, were fit by using the first-order rate law

$$A_{obsd} = A_\infty + \Delta A \exp(-k't) \quad (1)$$

in which A_∞, ΔA, and k' were adjusted to give the weighted least-squares fit of the data. In most cases both "fast" and "slow" first-order changes were observed which were separately fit by eq 1. The amplitude, ΔA, as a function of pH was fit first by eq 2 which is equivalent to an equation previously given

$$\Delta A_{obsd} = \frac{\Delta A_\infty + \Delta A_0 K_a/[H^+]}{1 + K_a/[H^+]} \quad (2)$$

by Johnson & Metzler (1970). The values of ΔA_∞ and ΔA_0, which represent the absorbance changes from the initial pH to infinite $[H^+]$ and zero $[H^+]$, respectively, were adjusted for best fit along with the apparent equilibrium constant, K_a. The final adjustment of the parameters for the model used in this paper is considered under Discussion.

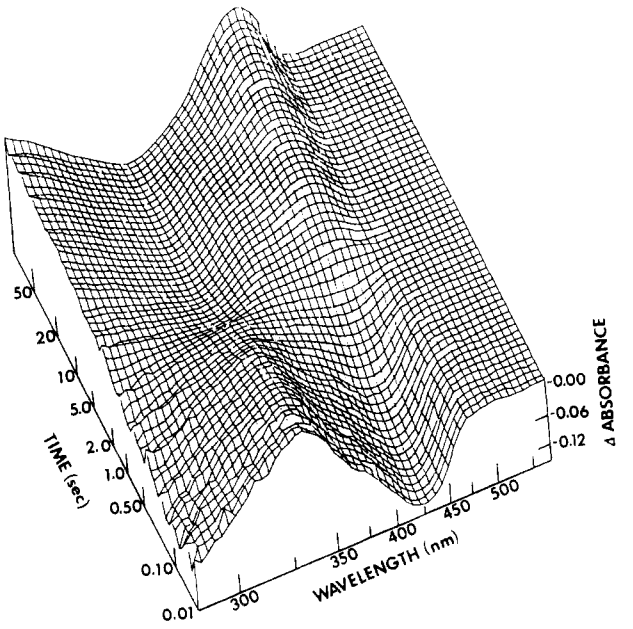

FIGURE 1: Three-dimensional surface showing the difference between absorbance as a function of wavelength and time and average absorbance at that wavelength. The data were recorded with a scanning stopped-flow spectrophotometer when the pH was dropped from pH 8.70 to 6.54. The conditions including enzyme concentrations are described under Materials and Methods.

pH Measurements. pH values were determined with a Beckman Model 4500 digital pH meter at 24 °C.

Results

As pointed out earlier, Morino & Snell (1967) originally showed that the 420-nm form of tryptophanase predominates at low pH values whereas at high pH values the 337-nm absorption predominates. The absorption spectra of tryptophanase at pH 7.00 and 9.33 obtained by scanning spectroscopy confirm these results (see corresponding spectra of Figure 10). To investigate the time-dependent interconversion of these spectral forms, the pH of an enzyme solution was increased (jumped) or decreased (dropped) in a scanning stopped-flow spectrophotometer and the absorbance was scanned as a function of wavelength and time as outlined under Materials and Methods. The overall spectral changes which occur during a pH-drop experiment are shown graphically in Figure 1 as a three-dimensional difference absorbance–wavelength–time surface. This presentation, which gives the difference between the absorbance at each wavelength and the average absorbance at that wavelength, emphasizes *changes* in absorbance during the reaction. This method of presentation gives a value of 0 at those wavelengths where no changes in absorbance occur. The data in Figure 1 clearly show the decay of the 337-nm peak,[2] growth of the 420-nm absorption, and the slow decay of absorption at 355 nm. This display also shows the increased noise level toward the UV end of the spectrum and the decrease in the relative noise level with time as a result of the averaging scheme used (Coolen et al., 1975).

Spectral changes in both the pH-jump and pH-drop experiments were analyzed in terms of three distinct phases: the first phase, an abrupt phase, is complete in <6.5 ms, the second

[2] For conformity with literature values, we will continue to use 337 and 420 nm as the wavelength maxima for the two absorption bands of bound pyridoxal phosphate even though the resolution of the scanning spectrophotometer does not exceed ±3 nm at 337 nm and ±4 nm at 420 nm at the settings used in these experiments.

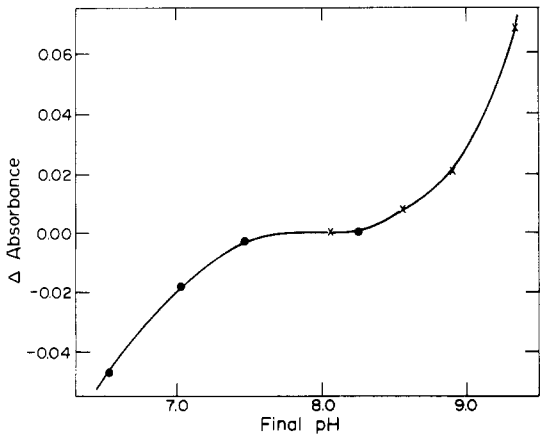

FIGURE 2: Change in absorbance at 295 nm as a function of pH obtained during the abrupt phase of incremental pH-jump (×) and pH-drop (●) experiments as described under Materials and Methods. The reference pH is 8.1.

phase involves a fast first-order interconversion of 420- and 337-nm absorbances, and the third phase is a slow first-order process involving growth at 335 nm coupled to two decays centered at 325 and 430 nm in the incremental pH jumps and decay at 355 nm with concomitant growth at 430 and 290 nm in the case of the incremental pH-drop experiments. Each of these phases will be discussed separately.

Abrupt Spectral Changes: First Phase. The first phase occurs during the 6.5-ms dead time of the stopped-flow instrument (with the 1.85 cm path length cell). The spectral changes occurring during this time are obtained by subtracting the spectrum of the enzyme at the initial pH (corrected for free pyridoxal-P absorption) from the spectrum taken immediately after the pH-jump or pH-drop (also corrected for free pyridoxal-P absorption). Thus each abrupt spectrum requires the comparison of four separate pushes taken at different times during a daylong run. A careful comparison of the abrupt spectral changes as a function of pH for both the pH-jump and pH-drop experiments shows small abrupt changes in absorbance above 330 nm ($\Delta A_{max} < 0.03$) (data not shown). Systematic but also small changes ($\Delta A_{max} = 0.07$ in the pH drop experiment) were observed near 295 nm. As shown in Figure 2, the absorbance in this region increases with increasing pH in a way which suggests the presence of a functional group with an apparent pK_a above 9, while the decreases in absorbance at 295 nm in the incremental pH-drop experiments are consistent with an apparent pK_a below 7.

Fast First-Order Interconversion of 420- and 337-nm Forms of Tryptophanase: Second Phase. A fast first-order interconversion of 420- and 337-nm absorbances occurs during the second phase. Figure 3 shows three representative difference spectra recorded during this second phase following an increase in pH from 7.00 to 9.33 (open symbols) and three following a decrease in pH from 8.70 to 6.54 (solid symbols). After a pH jump, there is a first-order growth centered at 330 nm coupled to first-order decays at 420 and 290 nm. The changes observed after a decrease in pH mirror those seen after a pH increase. Isosbestic points occur at 300 and 360 nm in both cases. Representative time-dependent growth and decay curves for one pH-jump experiment from pH 7.00 to 9.33, given in Figure 4, show that the changes occurring at 337 and 420 nm follow first-order kinetics.

The first-order rate constants and amplitudes for the changes in absorbance at 420 and 337 nm in the incremental pH-jump and pH-drop experiments were obtained by fitting the absorbance vs. time data at each wavelength to eq 1 with KINFIT4 (Dye & Nicely, 1971). They are available as

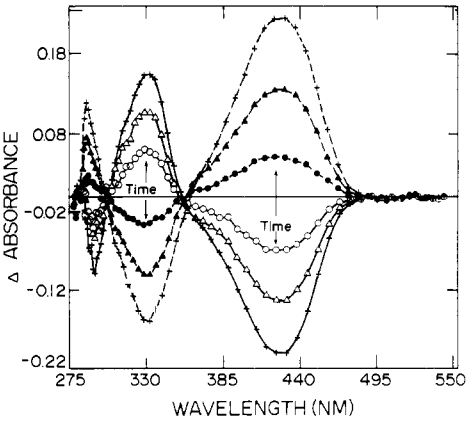

FIGURE 3: Difference spectra at three different times reflecting changes in absorbance observed during fast first-order interconversion of 420- and 337-nm forms after a jump in pH from pH 7.00 to pH 9.33 (○, △, +) and a drop from pH 8.70 to pH 6.54 (●, ▲, +). Each difference spectrum was obtained by subtracting the spectrum collected after completion of the abrupt phase from a succeeding spectrum at three different time points during the fast phase. The times at which each spectrum was recorded are, for the pH-jump experiment, (○) 0.16 s, (△) 0.4 s, and (+) 1.5 s and, for the pH-drop experiment, (●) 0.6 s, (▲) 2.5 s, and (+) 6 s. See Materials and Methods for details of the experiment.

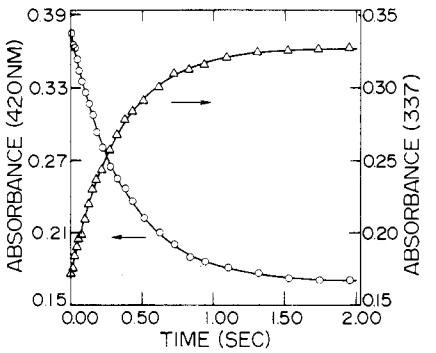

FIGURE 4: Changes in absorbance recorded at 420 (○) and 337 (△) nm as a function of time during the fast first-order phase following a jump in pH from pH 7.00 to pH 9.33 as described under Materials and Methods. Solid lines are for a first-order process with $k_1 = 2.63$ (○) and 2.78 (△) s^{-1}.

supplementary material (Appendix; see paragraph at end of paper regarding supplementary material). The adjustable parameters were A_∞, the absorbance at infinite time, ΔA, the change in absorbance (i.e., $(A_\infty - A_0)$, where A_0 is the absorbance at $t = 0$), and k_1, the apparent first-order rate constant. The rate constants for the changes in absorbance at both wavelengths were essentially the same for any one push but varied with pH in a systematic manner as indicated in Figure 5. The data for the changes centered at 290 nm appeared to show the same rate behavior as those at 337 and 420 nm, but the small amplitude of the changes at 290 nm and the greater noise at shorter wavelengths resulted in large standard deviations of the rate constants. The origin of the variation in k_1 as a function of pH, shown in Figure 5 as well as the equation for the calculated solid line through the data will be considered under Discussion.

The spectra after the fast first-order process following a pH jump to different final pH values are given in Figure 6. This figure clearly shows the pH-dependent conversion of the 420-nm absorption to the 337-nm species during this fast process. The amplitudes for the changes in absorbance at 420 and 337 nm during the fast process for both the pH-jump and pH-drop experiments are shown in Figure 7 as a function of pH. These absorbance changes for both pH jumps and pH drops have been normalized as described under Discussion.

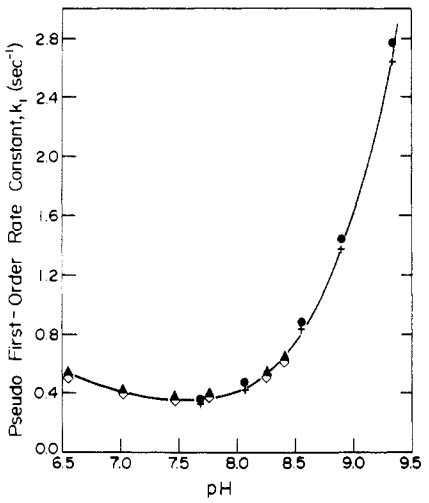

FIGURE 5: Pseudo-first-order rate constant for fast interconversion of 420- (+, ◊) and 337-nm (●, ▲) absorbances in the incremental pH jump (+, ●) and pH drop (◊, ▲) experiments plotted as a function of the final pH in each experiment. Each datum point represents the average of three experiments. The solid line was calculated with eq 6. See Materials and Methods for experimental details.

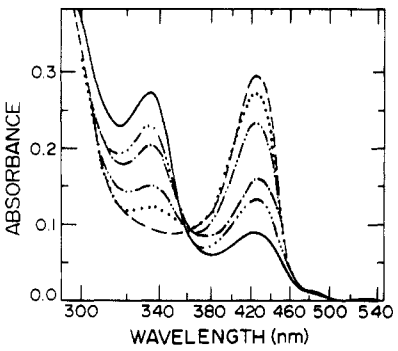

FIGURE 6: Final spectrum after completion of fast first-order interconversion of the 420- and 337-nm absorbances following a pH jump from pH 7 to pH 9.33 (—), pH 8.90 (-···-), pH 8.56 (-·-), pH 8.07 (-··-), and pH 7.69 (···) and at pH 7.0 (---). The absorbance of free pyridoxal-P has been subtracted.

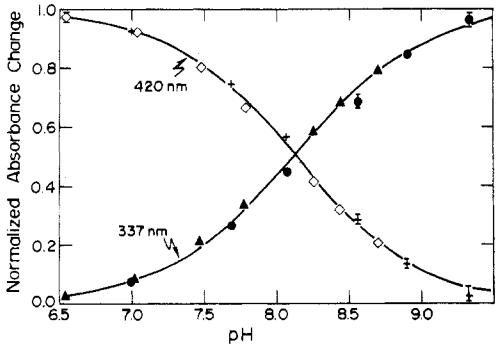

FIGURE 7: Plot of normalized change in absorbances at 337 and 420 nm observed during the fast second phase of pH-jump and pH-drop experiments. The normalization procedure is described under Discussion. Solid lines were calculated by eq 2, 3, 4, and 5. The meanings of the symbols are given in the legend to Figure 6.

The solid lines through the data represent the curves calculated from a least-squares fit of the data with the model also described under Discussion. The pH dependence of the amplitudes is defined well by a simple monoprotic titration curve with an apparent pK value of 8.11 ± 0.02.

Slow First-Order Processes: Third Phase. (*a*) *Incremental pH-Jump Experiments.* The changes in spectra which occur during the third phase of the pH-jump experiments from pH 7.00 to pH 9.33 are given in Figure 8. These changes involve

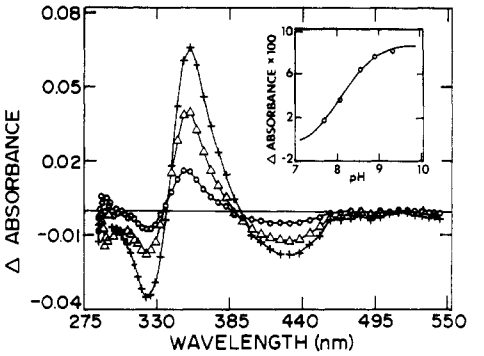

FIGURE 8: Difference spectra at three different times reflecting changes in absorbance observed during the slow first-order phase following completion of fast first-order interconversion of 337- and 420-nm absorbances after a pH jump from pH 7.00 to pH 9.33. Each difference spectrum was obtained by subtracting the spectrum collected after completion of the fast phase from a succeeding spectrum at three different times as follows: (○) 3.7 s; (△) 12 s; (+) 28 s. The inset presents the change in absorbance at 355 nm observed during the slow first-order process. The solid line was calculated with eq 2 by using pK = 8.10.

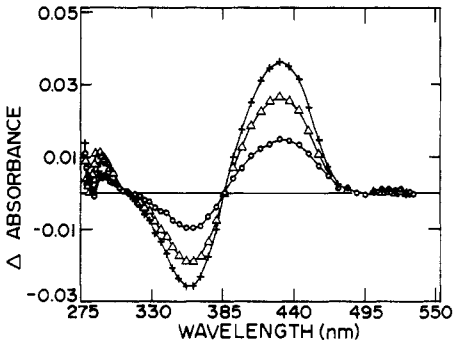

FIGURE 9: Difference spectra at three different times reflecting changes in absorbance observed during the slow first-order phase following completion of fast first-order interconversion of 337- and 420-nm absorbances after a pH drop from pH 8.70 to pH 6.54. The times were (○) 30, (△) 60, and (+) 110 s. The difference spectrum was obtained as indicated in legend of Figure 8.

growth at 355 nm with concomitant decays centered at 325 and 430 nm. Similar changes were observed at the four other final pH values. The absorbance vs. time data at the above three wavelengths were fitted by eq 1 to obtain values for A_∞, ΔA, and k_2, and are available as supplementary material (appendix, supplementary material). The rate constant for this slow third phase evaluated at 355 and 430 nm was independent of both wavelength and pH and gave an average value of 0.064 ± 0.005 s^{-1} for five determinations. Since the data at 325 nm were somewhat noisier and the amplitudes were generally smaller than those collected at the higher wavelengths, the rate constants at this wavelength are less well determined but appear to be somewhat smaller.

Although the amplitudes of the changes in absorbance at 325 and 430 nm were pH dependent, only those obtained at 355 nm were large enough at all pH values to analyze reliably. As indicated in the inset to Figure 8, the change in absorbance at 355 nm can be described by a simple monoprotic titration curve with pK = 8.1 ± 0.06. Thus, the amplitude of this slow process shows essentially the same pH dependence as the fast interconversion of the 420- and 337-nm forms of the enzyme in the pH-jump and pH-drop experiments.

(*b*) *Incremental pH-Drop Experiments.* Changes in spectra which occur during the third phase of the pH-drop experiments from pH 8.70 to 6.54 (Figure 9) involve a decay at 355 nm and growths at 430 and 290 nm. Similar changes were observed in five other experiments involving different pH spans.

Scheme I

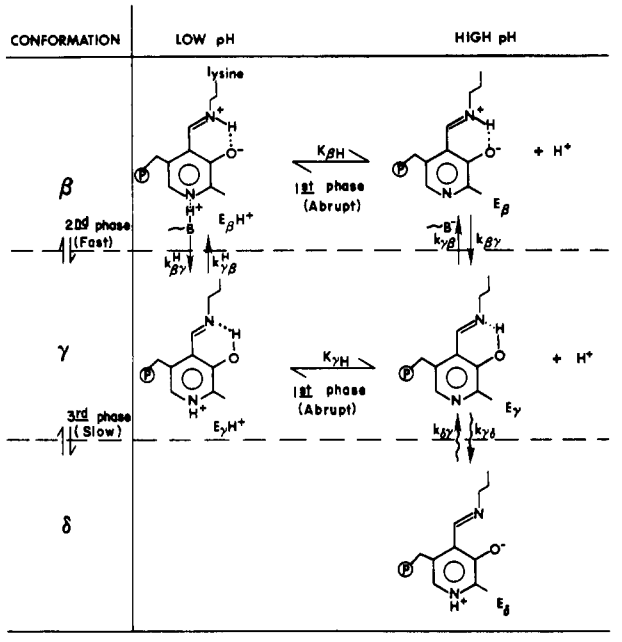

The changes at 290 nm, however, become negligible as the extent of the pH drop becomes smaller. The rate constants for the slow changes in the pH-drop experiments are substantially smaller than those obtained in the pH-jump experiments. The first-order rate constants for the change at 355 and 430 nm were 0.009 ± 0.004 and 0.008 ± 0.001 s^{-1}, respectively. As reflected in the standard deviations, these constants as well as the amplitudes are not well determined since data were collected for less than two half-lives.

When corrected for active enzyme concentration, the initial spectrum for the pH-drop experiments was the same, within experimental error (±0.005 *A*), as the final spectrum in a pH jump to the same pH except in the region of free pyridoxal-P absorption (390 nm) where the difference (0.03 *A*) is attributed to uncertainties in the spectrum of free pyridoxal-P (see Discussion).

Discussion

The data obtained in the pH-jump and pH-drop experiments as well as experiments described in the companion paper (June et al., 1981) are consistent with the model outlined in Scheme I for the holoenzyme in the presence of K^+. This scheme involves four enzyme conformations α, β, γ, and δ. Conformation α is the inactive holoenzyme which predominates in the absence of monovalent cations. This form also absorbs at 420 nm and is probably present as a minor species even in the presence of saturating concentrations of K^+. The other conformational forms or manifolds of forms are assigned on the basis of the different absorption maxima of the bound coenzyme.

The structures giving rise to these various absorptions are assigned on the basis of both model studies and studies on other pyridoxal-P-dependent enzymes (Matsushima & Martell, 1967; Johnson & Metzler, 1970). We propose that the two forms of coenzyme within the β and γ conformational manifolds differ only by their state of protonation at or near the pyridinium nitrogen. Protonation at this site does not greatly alter the position of the absorption maxima of pyridoxal-P Schiff bases although the extinction coefficients differ (Metzler et al., 1980). Both $E_\beta H^+$ and E_β would be expected to show an absorption maximum at ~420 nm, while the $E_\gamma H^+$ and E_γ absorptions would be centered at 337 nm.

Table I: Calculated Equilibrium Distribution[a] of Species in the β and γ Manifolds (Percent) as a Function of pH

pH	$E_\beta H^+$	E_β	E_γ	$E_\gamma H^+$
6.5	93.4	0.06	2.3	4.2
7.0	88.8	0.18	7.0	4.0
7.5	77.0	0.5	19.1	3.5
8.0	54.1	1.1	42.4	2.4
8.5	27.9	1.8	69.1	1.3
9.0	11.0	2.2	86.3	0.5
9.5	3.8	2.4	93.7	0.17

[a] This table is based upon enzyme in the β and γ manifolds only. It does not include contributions from the α and δ manifolds.

Table II: Best-Fit Parameters Based upon Scheme I and Their Marginal Standard Deviation Estimates

parameters	value	SD value	SD %
$(\epsilon_{\beta\beta_t}{}^0)_{jump}$	0.080 cm^{-1} [a]	0.001	1.4
$(\epsilon_{\beta\beta_t}{}^0)_{drop}$	0.0175 cm^{-1} [a]	0.0008	4.6
$(\Delta A_{337}/\Delta A_{420})$	−0.758	0.008	1.0
$K_{\beta H}$	2.0 × 10^{-10} M	0.4 × 10^{-10}	20
$K_{\beta\gamma}$	39	8	20
$K_{\gamma H}$	1.7 × 10^{-7} M	0.3 × 10^{-7}	18
$k_{\beta\gamma}$	8.3 s^{-1}	1.6	18
$k_{\beta\gamma_H}$	0.0297 s^{-1}	0.0045	15
K_a	7.7 × 10^{-9} M [b]	0.4 × 10^{-9}	5
$k_{\gamma\beta}$	0.212 s^{-1} [b]	0.012	6
$k_{\beta\gamma_H}$	0.045 s^{-1} [b]	0.010	20
$k_{\gamma\beta_H}$	0.66 s^{-1} [b]	0.4	6
ϵ_{420} for the [c] β form	4600 M^{-1} cm^{-1}	150	3.3
ϵ_{337} for the [c] γ form	3500 M^{-1} cm^{-1}	120	3.4

[a] Based on 1 mg mL^{-1} tryptophanase. [b] Calculated values from best-fit parameters given above. Standard errors calculated by propagation of error techniques. [c] Calculated from the first three entries in this table and based on an equivalent weight of 55 000. Standard errors calculated by propagation of error techniques. These values are calculated from the fast changes in absorbance at the indicated wavelengths for a change from $[H^+] = 0$ to $[H^+] = \infty$. Inclusion of the common background absorbances yields total extinction coefficients (in M^{-1} cm^{-1}) as follows: at $[H^+] = 0$, $\epsilon_{420}{}^0 = 7000$ and $\epsilon_{337}{}^0 = 2500$; at $[H^+] = \infty$, $\epsilon_{420}{}^\infty = 2500$ and $\epsilon_{337}{}^\infty = 5900$ (June, 1979).

Comparison of the difference spectra obtained during the abrupt phase of the pH-jump experiment (data not shown) with the calculated difference spectra of the Schiff bases of pyridoxal-P that are protonated or deprotonated at the pyridinium nitrogen [see Figure 1 of Metzler et al. (1980)] shows peaks and wells at roughly the same wavelengths. Using the molar difference absorptivities between the protonated and deprotonated Schiff bases estimated from Figure 1 of Metzler et al. (1980), we would expect a value of $\Delta A = +0.05$ at 270 nm and −0.05 at 420 nm during the abrupt phase of a pH-jump experiment in which the pH was jumped from 7 to 9.33. We observed $\Delta A = +0.07$ at 295 nm and $\Delta A = -0.03$ at 420 nm. The expected values were calculated by assuming that 90% of the enzyme exists in the βH^+ form at pH 7.00 (Table I) and that $pK_{\beta H} = 9.7$ (Table II). Because of the uncertainties of comparing spectra of solution and enzyme-bound pyridoxal-P Schiff bases and because of the technical difficulties of obtaining small spectral changes during the abrupt phase, especially in the presence of excess pyridoxal phosphate (see Results), we would expect an uncertainty of at least ±0.02 *A*. The pH dependence of the changes at 295 nm during the abrupt phases of the pH-jump and pH-drop experiments (Figure 2) is consistent with a $pK_{\beta H} = 9.7$ and a $pK_{\gamma H} = 6.8$ (Table II). These p*K* values were calculated from independent data as described later under Discussion. Since we expect a p*K* near 6.4 for the pyridinium nitrogen of Schiff bases

(Metzler et al., 1980), a group, BH^+, was added in Scheme I that interacts with the pyridinium nitrogen of the β form to account for the observed $pK = 9.7$. We also assume that the proposed conformation change leading to the γ form destroys the interaction of the B group resulting in a pyridinium nitrogen with a $pK = 6.8$. The interaction of the B group with the pyridinium nitrogen is preferred since other evidence (June et al., 1981) indicates that the substrate interacts with the βH^+ form resulting in the transaldimination reaction. The subsequent formation of a quinonoid requires a protonated pyridinium nitrogen. It should be emphasized, however, that other forms of the coenzyme such as that suggested by O'Leary & Brummond (1974) may also be consistent with the data.

The structure of the coenzyme in E_δ which absorbs at 355 nm was assigned on the basis of studies done with aspartate aminotransferase where a 360-nm form of the coenzyme is associated with activity (Ivanov & Karpeisky, 1969) and also on the basis of the spectra of model compounds (Metzler et al., 1980). This may be the form of the coenzyme in tryptophanase which can be photoinactivated since the maximal rate of inactivation occurs at a similar wavelength (Coetzee & Pollard, 1975).

The pH dependence of the fast pseudo-first-order rate constant, k_1, and the amplitudes of the absorptions at 337 and 420 nm are attributed to a pH-dependent conformational change which involves interconversion of the β and γ "manifolds". The conversion of β, which absorbs at 420 nm, to γ, which absorbs at 337 nm, may result from an increase in the hydrophobicity at the coenzyme site, presumably as a result of a conformational change. Indeed, the relative intensities of bands at 420 and 337 nm have been used as a measure of the hydrophobic nature of the environment of pyridoxal-P (Llor & Cortijo, 1977; Cortijo et al., 1978).

Qualitatively, the dependence of k_1 on pH shown in Figure 5 results from the presence of two pathways for equilibration of the β and γ manifolds. Since $pK_{\beta H}$ is high ($\sim$9.7), the apparent rate increases with increasing pH as the concentration of E_β becomes larger. As the pH is lowered, protonation of E_γ begins to become important ($pK \simeq 6.8$) and the two manifolds equilibrate via the interconversion of $E_\beta H^+$ and $E_\gamma H^+$.

The β to γ conversion described by Scheme I involves five independent equilibrium and rate constants and three independent amplitude terms. To evaluate these eight constants, we have available the pH dependence of the changes in absorption amplitude at 337 and at 420 nm and the pH dependence of the pseudo-first-order rate constant k_1. As outlined in the supplementary material, the amplitude of the change in absorbance with pH at 420 nm during the fast process can be described by eq 2 in which

$$\Delta A_\infty = \frac{(\epsilon_\beta \beta_t^0)(K_{\gamma H} - K_{\beta H})}{\left(1 + \frac{K_{\gamma H}}{K_{\beta H} K_{\beta\gamma}}\right)(K_{\beta H} + [H^+]_0)} \quad (3)$$

$$\Delta A_0 = \frac{(\epsilon_\beta \beta_t^0)[H^+]_0 (K_{\beta H}/K_{\gamma H} - 1) K_{\beta\gamma}}{(1 + K_{\beta\gamma})(K_{\beta H} + [H^+]_0)} \quad (4)$$

$$K_a = \frac{K_{\beta H}(1 + K_{\beta\gamma})}{1 + K_{\beta H} K_{\beta\gamma}/K_{\gamma H}} \quad (5)$$

The equilibrium constants are defined by Scheme I. The change in absorbance at 337 nm is of opposite sign but proportional to that at 420 nm. The three adjustable amplitude parameters are, then, $(\epsilon_\beta \beta_t^0)_{jump}$, $(\epsilon_\beta \beta_t^0)_{drop}$, and $\Delta A_{337}/\Delta A_{420}$. The terms $(\epsilon_\beta \beta_t^0)_{jump}$ and $(\epsilon_\beta \beta_t^0)_{drop}$ represent the contribution of the mixture of $E_\beta H^+$ and E_β to the 420-nm absorbance at the respective initial pH values. This is in addition to the background absorbance common to both the β and γ manifolds (see Figure 10).

As described in the supplementary material, the pH dependence of the pseudo-first-order rate constant is given by

$$k_1' = \frac{k_{\beta\gamma} K_{\beta H} + k_{\beta\gamma}{}^H [H^+]}{K_{\beta H} K_{\beta\gamma}(1 + [H^+]/K_{\gamma H})} + \frac{k_{\beta\gamma}{}^H + k_{\beta\gamma} K_{\beta H}/[H^+]}{1 + K_{\beta H}/[H^+]} \quad (6)$$

Thermodynamic constraints require that

$$K_{\beta\gamma}{}^H = K_{\beta H} K_{\beta\gamma}/K_{\gamma H} \quad (7)$$

and, of course

$$k_{\gamma\beta} = k_{\beta\gamma}/K_{\beta\gamma} \quad (8)$$

and

$$k_{\gamma\beta}{}^H = k_{\beta\gamma}{}^H/K_{\beta\gamma}{}^H \quad (9)$$

For evaluation of the eight independent parameters, the amplitude data at 337 and 420 nm for both the pH-jump and pH-drop experiments together with all of the pseudo-first-order rate constants were *simultaneously* fit by using the nonlinear least-squares program KINFIT4 [adapted from Dye and Nicely (1971)]. All data were individually weighted by using statistical information from triplicate sets of pushes. Convergence to a true minimum was tested by using two calculations having initial estimates of the parameters which bracketed the final values. The solid curves in Figures 5 and 7 are calculated from the best-fit parameters. In order to present all of the amplitude changes given in Figure 7 on a single graph, we first added the observed values of ΔA_{337} and ΔA_{420} (with the appropriate sign) to the *calculated* absorbance change for a pH drop from $[H^+] = 0$ to the initial pH of the experiment. This sum was then divided by the calculated absorbance change for a pH drop from $[H^+] = 0$ to $[H^+] = \infty$. The values of all eight parameters and their marginal standard deviation estimates as well as the calculated values of the derived parameters K_a, $K_{\beta\gamma}{}^H$, $k_{\gamma\beta}$, and $k_{\gamma\beta}{}^H$ with their computed uncertainties are given in Table II. By use of these values, the computed equilibrium distributions among the four species $E_\beta H^+$, E_β, E_γ, and $E_\gamma H^+$ as a function of pH are given in Table I. It can be seen that over the accessible pH range, the two species $E_\beta H^+$ and E_γ predominate. This means that any errors in the assumption that $E_\beta H^+$ and E_β have the same extinction coefficient (and the similar assumption about $E_\gamma H^+$ and E_γ) have minimal detrimental effect. The calculated molar extinction coefficients of the β and γ forms at the wavelengths of their respective maxima are also given in Table II. This calculation assumes that the concentration of the α and δ forms are insignificant at the pH extremes.

The conformational manifold which contains the species designated as E_δ was added to account for the changes in the spectrum observed during the slow first-order process in both the pH-jump and pH-drop experiments. Because the rates of formation and disappearance of E_δ are slow compared to the equilibration time of the β and γ manifolds, it is not possible to determine which of the four species $E_\beta H^+$, E_β, E_γ, or $E_\gamma H^+$ is directly converted to E_δ. Indeed, it is even possible that E_δ is formed from the inactive enzyme, E_α. The pH dependence of the amplitude shows that E_δ is one proton removed from $E_\beta H^+$ (and $E_\gamma H^+$), at least insofar as medium protons are concerned. The slow changes in the spectra above 315 nm after a pH jump can be quantitatively accounted for by a decrease in the concentrations of E_γ (337 nm) and E_β plus E_α (420 nm) and the growth of a species with maximum absor-

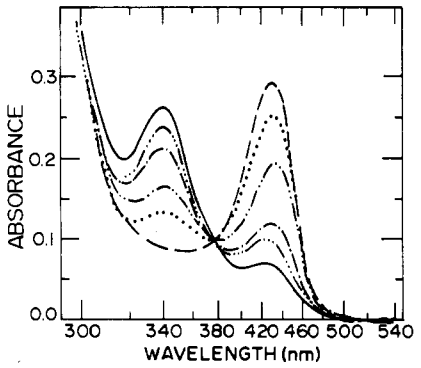

FIGURE 10: Final absorption spectra of tryptophanase after completion of all changes following a jump in pH from pH 7.00 to pH 9.33 (—), pH 8.90 (-···-), pH 8.56 (-·-), pH 8.07 (-··-), and pH 7.69 (···) and at pH 7.00 (---). The absorbance of free pyridoxal-P has been subtracted.

bance at ~355 nm (E_δ). The magnitude of the change suggests that E_δ is not a major species. However, the equilibrium ratio $[E_\delta]/[E_\gamma]$ could be as large as 0.5.

The observed rate constant for the formation of E_δ appears to be independent of pH, but the amplitude is strongly pH dependent (supplementary material, appendix). In addition, the rate of disappearance of E_δ in the pH-drop experiments is ~8 times slower than its rate of appearance after a pH jump. All of these facts suggest that the formation of E_δ is not a simple one-step reaction connected with any of the species in the β or γ manifold. The effect of buffer components may also be important. In a similar study on the pyridoxal-dependent enzyme glutamate decarboxylase, O'Leary & Brummond (1974) observed that the rate of conversion of a species absorbing at 420 nm following a rapid decrease in pH was affected by the nature and concentration of the buffer used. It is conceivable that the rate of formation and disappearance of the manifold is also sensitive to buffer effects. Additional experiments under various buffer conditions will be required to answer this question.

The spectral peak remaining at 420 nm after the fast first-order process following a pH jump from 7.00 to 9.33 (Figure 6) is larger than predicted on the basis of the concentration of species in the β manifold at this pH. The excess absorbance above a smooth base line corresponds to ~25% residual absorbance at 430 nm whereas the equilibrium constants given in Table II suggest that only ~8% of the β manifold is present at this pH. Therefore, we conclude that ~17% of the enzyme at pH 7.00 is present as conformation α which also absorbs at 420 nm and is only slowly converted into the other species. The final spectra after the slow process following a pH jump are shown in Figure 10. The final absorbance at 430 nm after a pH jump from 7.00 to 9.33 corresponds to ~15% of the initial absorbance suggesting that some of the α manifold is still present at equilibrium. It will be necessary to study the conversion of inactive to active enzyme in order to obtain further information about the α and δ conformations.

The abrupt spectral changes described in this paper differ, particularly in the magnitude of the change, from the abrupt changes described in a preliminary report of this work (June et al., 1979). Although the initial spectrum shown in Figure 1 of June et al. (1979) agrees with the present results, the abrupt and final spectra shown in this figure are different. The differences are well beyond our instrumental error and suggest that the spectrum of "free" pyridoxal-P in the presence of fully saturated holoenzyme is not the same as that in the absence of enzyme and probably depends upon enzyme concentration, pH, and the length of time between preparation and use. Subsequent experiments (data not given) show that excess pyridoxal-P binds to the enzyme at some site other than the active site and also interacts with DTT with a change in spectrum. These problems add to the difficulty of assessing the magnitude of the abrupt spectral changes observed in these experiments.

Acknowledgments

We thank Iraj Behbahani-Nejad for assistance with the calculations and Professor A. El Bayoumi for constructive suggestions and discussions.

Supplementary Material Available

An appendix of the derivation of equations which describe the rate of interconversion of the β and γ manifolds and the final relative concentrations of the four species βH^+, γH^+, β, and γ and tables of rate constants and amplitudes for the fast first-order interconversion of the 420- and 337-nm absorbances in the incremental pH-jump and -drop experiments and for the slow first-order processes at 325, 355, and 430 nm, in the incremental pH-jump experiments (5 pages). Ordering information is given on any current masthead page.

References

Coetzee, W. F., & Pollard, E. C. (1975) *Photochem. Photobiol. 22*, 29–32.

Coolen, R. B., Papadakis, N., Avery, J., Enke, C. G., & Dye, J. L. (1975) *Anal. Chem. 47*, 1649–1655.

Cortijo, M., Jimenez, J. S., & Llor, J. (1978) *Biochem. J. 171*, 497–500.

Dye, J. L., & Nicely, V. A. (1971) *J. Chem. Educ. 48*, 443–448.

Hogberg-Raibaud, A., Raibaud, O., & Goldberg, M. E. (1975) *J. Biol. Chem. 250*, 3352–3358.

Ivanov, V. I., & Karpeisky, M. Y. (1969) *Adv. Enzymol. Relat. Areas Mol. Biol. 32*, 21–53.

Johnson, R. J., & Metzler, D. E. (1970) *Methods Enzymol. 18A*, 433–471.

June, D. S. (1979) Ph.D. Dissertation, Michigan State University, East Lansing, MI.

June, D. S., Kennedy, B., Pierce, T. H., Elias, S. V., Halaka, F., Behbahani-Nejad, I., El Bayoumi, A., Suelter, C. H., & Dye, J. L. (1979) *J. Am. Chem. Soc. 101*, 2218–2219.

June, D. S., Suelter, C. H., & Dye, J. L. (1981) *Biochemistry* (following paper in this issue).

Llor, J., & Cortijo, M. (1977) *J. Chem. Soc., Perkin Trans. 2*, 1111–1113.

Matsushima, Y., & Martell, A. E. (1967) *J. Am. Chem. Soc. 89*, 1322–1330.

Metzler, C. M., Cahill, A., & Metzler, D. E. (1980) *J. Am. Chem. Soc. 102*, 6075–6082.

Morino, Y., & Snell, E. E. (1967) *J. Biol. Chem. 242*, 5591–5601.

O'Leary, M. H., & Brummund, W., Jr. (1974) *J. Biol. Chem. 249*, 3737–3745.

Papadakis, N., Coolen, R. B., & Dye, J. L. (1975) *Anal. Chem. 47*, 1644–1649.

Snell, E. E. (1975) *Adv. Enzymol. Relat. Areas Mol. Biol. 42*, 287–333.

Suelter, C. H., Coolen, R. B., Papadakis, N., & Dye, J. L. (1975) *Anal. Biochem. 69*, 155–163.

Suelter, C. H., Wang, J., & Snell, E. E. (1976) *FEBS Lett. 66*, 230–232.

Suelter, C. H., Wang, J., & Snell, E. E. (1977) *Anal. Biochem. 76*, 221–232.